Shear-Induced Demixing and Shear-Banding Instabilities in Dilute Triblock Copolymer Solutions

G. Waton, B. Michels, A. Steyer, and F. Schosseler*

Laboratoire de Dynamique des Fluides Complexes, UMR 7506, 4 rue Blaise Pascal, 67070 Strasbourg Cedex, France

Received July 3, 2003; Revised Manuscript Received January 12, 2004

ABSTRACT: We study dilute aqueous solutions of a triblock copolymer PEO−PPO−PEO (Pluronics P84) by rheometry coupled with small-angle light scattering. The zero-shear viscosity increases by 5 orders of magnitude upon increase of temperature from 30 to 40.5 °C. This increase can be explained by the growth of spherical micelles to entangled cylindrical aggregates. In the non-Newtonian regime, we find evidence for shear-induced demixing below 37.7 °C and for gradient shear banding above this temperature. Thus, above a critical temperature the shear-induced demixing triggered by the flow in the vicinity of the cloud point (43 °C) appears linked to a phase separation of regions with different shear rates. At fixed concentration, the control parameters of the dynamic phase diagram are the temperature and the flow.

I. Introduction

Pluronics, also termed Poloxamers or Synperonics, are block PEO−PPO−PEO copolymers of poly(ethylene oxide) (PEO) and poly(propylene oxide) (PPO). The solubility of PPO blocks exhibits dramatic temperature dependence in aqueous solutions. At low temperature, the water is a solvent for PPO whereas at high temperature the PPO is not soluble in aqueous solutions. The PEO is soluble in the temperature range 0−100 °C. Pluronics have numerous industrial uses, especially in the pharmaceutical industries.[1] Their hydrophilic/hydrophobic balance can be varied by changing the PEO/PPO molar ratio and the temperature.[1] Under suitable conditions, these triblock molecules aggregate in aqueous solutions forming multimolecular micellar aggregates. In these micelles, the hydrophobic blocks constitute the core and the hydrophilic blocks along with the water form the corona. The critical micellar concentration (cmc) at a given temperature or the critical micellar temperature (cmT) at constant concentration can be varied by changing the PEO/PPO molar ratio and the total molecular weight.[1,2] The solution behavior of Pluronics solutions is therefore of both applied and fundamental physicochemical interest.

The properties of Pluronics solutions have been extensively investigated using techniques such as microcalorimetry,[3−10] small-angle neutron or X-rays scattering,[2,10−18] static[19,20] and dynamic[19,21−23] light scattering, or rheometry.[5,9,19,22,24] The variation of the critical micelle concentration (cmc) with molecular weight, temperature, or salt concentration is widely studied using the microcalorimetry technique. The main results are the decrease of cmc when temperature or monovalent salt concentration increases and when the PEO/PPO ratio decreases. The structure of the micelles are best investigated using scattering techniques. At concentrations above the cmc (or temperatures above the cmT) the micelles are spherical. At low temperature many water molecules are present in the micelle core, and when temperature increases the hydration of the core decreases while the aggregation number increases.[14]

Far from the cmT and in the concentrated regime (typically above 0.2 weight fraction), the micelles can form ordered structures due to the close packing.[17,18] The solutions become highly viscous or even exhibit gellike behaviors.[19] The rheological properties in this regime have been widely investigated, and a number of interesting phenomena like yield stress,[15] banded flow,[15,16] layer sliding,[12] and glassy behavior[23] have been reported for various systems.

The rheological properties in the dilute regime, for concentrations typically below 0.1 weight fraction, have received much less attention. While many studies have reported the linear viscoelastic properties of dilute solutions for the purpose of establishing temperature−concentration phase diagrams, no detailed investigation of the rheological properties in the non-Newtonian regime has been published, as far as we know, for the dilute concentration regime.

In the dilute regime, increasing the temperature from the cmT at constant concentration results in an increase of the relative viscosity by a factor about 5.[24] This increase has been successfully described[24] by a model of sticky hard spheres, the stickiness parameter being deduced from independent SANS experiments. On the other hand, structural studies by scattering techniques have evidenced a rodlike behavior of the aggregates at higher temperatures in dilute solutions.[2,5,10,13,19,22] More recently, microcalorimetry experiments in this regime have detected micellar growth correlated with a large increase of the relative viscosity measured with a capillary viscometer.[9] Thus, it seems that at temperatures close to (but still above) the cmT a short-range attractive contribution driving the self-association of spherical micelles can explain the viscosity increase. This mechanism would favor above some critical concentration a percolating network of micelles with increasing strength as the temperature increases. However, the parallel increase of the aggregation number and the dehydration of the core with increasing temperature[14] play a decisive role by changing the interface curvature and driving a change of micellar morphology from spheres to spherocylinders. This growth induces much more dramatic effects.

In the present study we focus on moderate weight fraction (0.04) Pluronics solutions at temperatures higher than the temperature associated with the mi-

10.1021/ma0349332 CCC: $27.50
Published on Web 02/14/2004

cellar growth. Therefore, we expect the micelles to be more or less entangled depending on their temperature-dependent equilibrium average length. First, by means of strain step and oscillatory measurements, we investigate the linear rheology of solutions at thermodynamic equilibrium to check the consistency of the solution properties with the picture of more or less entangled spherocylinders. Second, using a combination of rheometry with small-angle light scattering, we study these solutions under steady shear flow as a function of shear rate and enter in the non-Newtonian regime where the flow strongly perturbs the structure of the solution and where no experimental results on such systems are yet available.

II. Experimental Section

Samples. We used without further purification Pluronics P84 supplied by BASF. The total molecular weight is 4200, and the nominal stoichiometry is $PEO_{19}-PPO_{43}-PEO_{19}$. In the absence of added salt, the cmT and the cloud point temperatures are around 20 °C and 75 °C, respectively. Salt addition is a convenient method to shift downward these temperatures (salting-out effects).[22] We have chosen to study samples in the presence of 2 M NaCl. At this salt concentration, the microcalorimetric measurements[9] show that, for a 4% w/w concentration, the cmT and the cloud point are at about 2 °C and 43 °C, respectively, and that the peak in the thermograms associated with the viscosity enhancement is shifted down from 55 °C to about 30 °C. In this temperature range, the temperature regulation of the solution is easier and the evaporation is minor. Stock solutions were prepared and then stored in the dark at 4 °C for further use. Reproducibility of the preparation was checked by differential scanning microcalorimetry.

Rheo-SALS. Simultaneous measurements of the rheological properties and of the small-angle light scattering (SALS) intensity have been performed using concentric cylinders geometry (Couette). A full description of the optical setup, of the calibration procedures, and of the treatment of intensity data has been given elsewhere.[25] The apparatus described in this reference has been improved by replacing the previous actuating device by a regular rheometer (Thermo Haake, RS1) on which a home-built thermostated cell was installed. The two concentric cylinders of the scattering cell are made of 2 mm thick Suprasil quartz and have inner radii of 24 and 27 mm, thus allowing for a 1 mm wide shearing gap, with a height along the vorticity direction about 60 mm. Compared to the previous setup, the inner cylinder is rotating and the outer static cylinder is surrounded by a cylindric bath with circulating water. Two windows in the bath clear the path for the entrance of the laser beam (incident wavelength 488 nm) and for the scattered light. By convention, in the following, the velocity is along the x axis, the velocity gradient along the y axis, and the vorticity along the z axis. The incident beam is along the velocity gradient direction and the scattering intensity is measured in the velocity−vorticity plane. The illuminated volume is approximately cylindrical across the gap with a length of 1 mm (size of the gap) and a diameter about 80 μm. The scattering volume depends on the scattering angle: [25] it is the whole illuminated volume at the smallest scattering angle, around 1°, and about one-third of the illuminated volume at the largest scattering angle around 10°. This means the scattering intensity measured at the detector collects the contributions from different points across the gap: in particular, in the case of shear gradient banded flows, contributions from layers with different shear gradient are superposed. The temperature is measured by a Pt probe located inside the massive aluminum base of the bath. The rheometer is by construction a stress-controlled device but can be operated by software in the shear-controlled mode, allowing a great versatility in experiments. Inertia corrections have been applied when necessary. The zero shear viscosity was measured in the stress-controlled mode ($\sigma = 0.2$ Pa). Step strain experiments were done in the constant deformation mode of the instrument. We checked that the nominal values for the strain γ were obtained for the first measured point of the relaxation modulus obtained for an elapsed time about 0.17 s. Oscillatory shear measurements were done in the stress-controlled mode with a constant applied stress $\sigma = 0.2$ Pa.

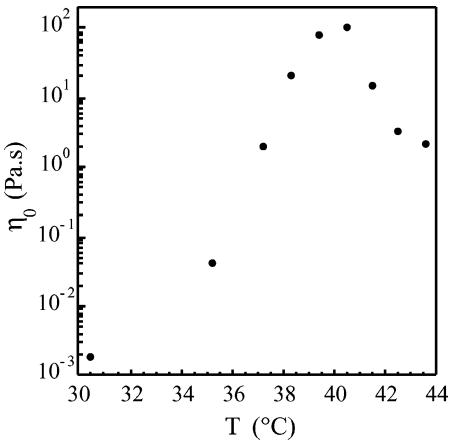

Figure 1. Evolution of the zero-shear viscosity η_0 with temperature.

The measurements of the flow curves were always performed according to the same procedure in sequences of increasing shear rates. A fresh sample from the stock solution was loaded into the Couette and then brought in one step to the temperature studied. The sample was left 1 h at rest at this temperature to allow for a reasonable thermal equilibrium of the whole setup. The measured fluctuations of temperature around the mean value were then about ±0.03 °C during the whole experiment. Shear rate values below 0.08 s^{-1} were achieved in the stress-controlled mode while higher values were measured by imposing the shear rate value. Steady-state values for the shear rate $\dot{\gamma}$ or the shear stress σ were obtained in typically 1 min, except for the lowest shear rates where times to reach the steady state could be as large as 10 or 20 min. At least 10 min of steady-state behavior was allowed before the measured shear rate or shear stress was considered meaningful, and a stack of typically 100 scattering intensity frames (exposure time 1 ms), separated by 0.5 s intervals, was recorded. Spurious frames contaminated by stray light originating from digs and scratches in the Couette walls were discarded (typically none to about 20% of the frames). The remaining frames were averaged to obtain an ensemble average of the intensity scattered from the sheared sample. Absolute intensity calibration was achieved by measuring a dilute solution of latices as described in ref 25.

III. Results

A. Linear Regime. 1. Zero-Shear Viscosity. The zero-shear viscosity η_0 of the solutions exhibits a huge variation over 5 orders of magnitude as the temperature T increases from 30 to 44 °C (Figure 1). It is close to the solvent viscosity in the range 20 °C to about 33 °C, which is the temperature where DSC experiments have revealed a small endothermic peak that was attributed to the onset of micellar growth.[9] At this temperature, the zero-shear viscosity increases steadily to reach a maximum value of the order of 100 Pa s at a temperature around 41 °C before decreasing as the temperature is further raised to 44 °C. Turbidity measurements show[9] that the cloud point is close to 43 °C and that for higher temperatures the turbidity increases with time, thus confirming the onset of a slow phase transition in this temperature regime. Therefore, in the following we have restricted our temperature variation to the window where the quiescent system can be considered to be close to a thermodynamic equilibrium.

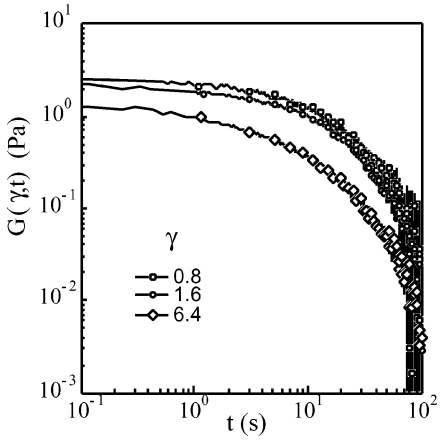

Figure 2. Shear relaxation modulus $G(\gamma,t)$ measured at $T = 40.5$ °C for different step strain amplitudes γ. For the sake of readability, only one point out of 20 is figured, and the time scale has been limited to 100 s although the data extend up to 250 s.

It is worth emphasizing that the $\eta_0(T)$ curves display some sensitivity to the thermal history of the samples. In particular, the curves can be slightly shifted along the temperature axis if the samples are brought suddenly from room temperature to temperatures above 35 °C or if the temperature is progressively increased by 1 °C steps with an equilibrium time of 10 min between each step. The maximum shifts we have observed correspond to less than 1 °C in the position of the viscosity maximum. Therefore, we can assert reasonably $T_{max} \approx 40.5 \pm 1$ °C. On the other hand, when plotted as a function of $T - T_{max}$, the viscosity curves superpose satisfactorily.

2. Relaxation Modulus. Typical curves for the shear relaxation modulus obtained through step strain experiments are shown in Figure 2. They are usually characterized by a fast decay at short times followed by an exponential decay at times longer than a few seconds. Experiments performed with varying strain amplitudes have shown that the fast relaxation depends on the strain amplitude γ and seems to vanish for very small γ values while the time constant of the exponential decay is independent of γ. In fact, it is possible to superpose the long time tails of curves corresponding to different γ by a vertical shift.

This suggests that for long times the relaxation modulus $G(\gamma,t)$ can be factorized as $G(\gamma,t) = h(\gamma)\, G(t)$ as in the case of polymer systems.[26,27] Here $G(t)$ is the linear relaxation modulus, and $h(\gamma)$ is the so-called damping function that describes the change upon a step deformation in the orientational distribution function of tangent unit vectors along the chains.[27] For entangled polymer systems, a step deformation results in a stretching and an orientation of the chains. The stress relaxation occurs through both the retraction of the stretched chains within their confining tube (characteristic time τ_R) back to their equilibrium end-to-end distance and the reptation of the orientated chains out of their confining tube (characteristic time τ_d). At times larger than the Rouse relaxation time τ_R, the stretching of the chains has completely relaxed, and only the randomization of the orientation still proceeds through the reptation mechanism. Thus, the temporal decay at times larger than τ_R should be independent of the amplitude of the initial stretching, i.e., of γ. This explains qualitatively the factorization of $G(\gamma,t)$ at long times, a result that can be justified analytically as well.[27] For polymer solutions, plots of $G(\gamma,t)/h(\gamma)$ indeed superpose for times larger than the Rouse relaxation time τ_R,[26,27] and $h(\gamma)$ has been found independent of polymer concentration and molecular weight in very good agreement with the predicted values.[26] Since the analogy with semidilute polymer solutions has been fruitful to understand the structure, the dynamics, and the rheology of short surfactant wormlike micelles in solution, we proceed with the same analogy here.

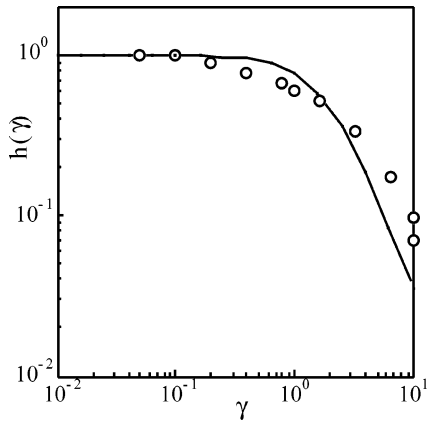

Figure 3. Plot of the damping function $h(\gamma)$ measured at $T = 40.5$ °C. The continuous line is the Doi−Edwards prediction for entangled polymer solutions.

Figure 3 compares the $h(\gamma)$ values obtained for our systems with the theoretical prediction by Doi−Edwards.[27] The two curves show clearly distinct behaviors, suggesting that the long entangled wormlike micelles presumably constituting our solutions do not behave like flexible polymers upon a sudden strain. In particular, it is clear that the nonlinear behavior appears for γ values as small as 0.2 for $T = 40.5$ °C. A similar early departure from linear regime was also observed in small surfactant solutions.[28] At this temperature, for γ values smaller than 0.2, the measured relaxation modulus appears independent of γ within the large experimental noise and should correspond to the linear relaxation modulus $G(t)$. It appears that it can be fitted as a single exponential with an adjustable baseline. In these conditions, the corresponding plateau modulus at $T = 40.5$ °C is found to be $G_0 \approx 2.6 \pm 0.2$ Pa. We have to emphasize that the experimental noise prevents us to conclude unambiguously about the single-exponential behavior of the linear relaxation modulus. For other temperatures step strain experiments in the linear regime are rather difficult due to the limited sensitivity of the rheometer, and the situation is even worse. In practice, for most of the solutions away from T_{max}, we used γ values already in the nonlinear regime and analyzed only the long time exponential tail to extract a characteristic time τ that was checked to be independent of γ. For all these temperatures we cannot elaborate further about the analytical form of $G(t)$ (see however next part). Figure 4 shows that the characteristic time τ values lie between 1 and 25 s depending on T and exhibit a variation similar to that of the zero-shear viscosity as the temperature is varied. From these data, it can be inferred that the plateau modulus $G_0 \sim \eta_0/\tau$ is also displaying a similar behavior (not shown in the figure).

3. Storage and Loss Moduli. Oscillatory shear measurements in the linear regime are shown in Figure 5 for some temperatures. The moduli G' and G'' exhibit the characteristic behavior of viscoelastic liquid al-

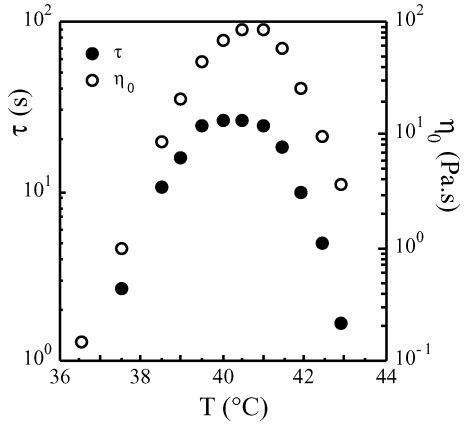

Figure 4. Evolution of the relaxation time τ and of the zero-shear viscosity η_0 with temperature.

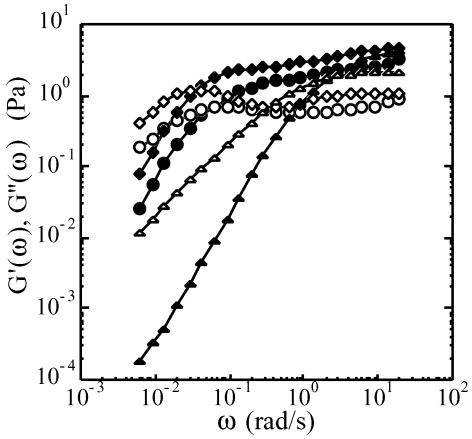

Figure 5. Frequency dependence of the storage (closed symbols) and loss (open symbols) moduli for some temperatures: circles, $T = 38.6$ °C; diamonds, $T = 40.5$ °C; triangles, $T = 42.5$ °C. Lines are guides for the eye.

though the limited experimental range does not allow to explore the terminal behavior for most of the temperatures. We can define a characteristic relaxation time $\tau_c = \omega_c^{-1}$, where ω_c is the pulsation where $G'(\omega)$ and $G''(\omega)$ intersect. This characteristic time τ_c is in good numerical agreement with the relaxation time τ obtained from the step strain experiments and displays the same behavior as a function of temperature. These samples never exhibit a plateau behavior for the storage modulus $G'(\omega)$ that would be characteristic for a gel. The typical curves in Figure 5 illustrate that it would be meaningless to try to determine a sol−gel transition boundary in these systems by following the temperature evolution of the storage modulus at a fixed frequency, whatever this frequency: the shift of the characteristic time with temperature prevents one to find a frequency that would correspond to some plateau regime of $G'(\omega)$ for the whole temperature range.

Interestingly, the $G'(\omega)$ vs $G''(\omega)$ plots (so-called Cole−Cole plots) do not appear as regular semicircles at all temperatures except for T_{max} where the semicircular shape is more closely followed. This means that, except maybe for T close to T_{max}, these systems cannot be considered as Maxwellian fluids. In this respect, we expect that a single-exponential behavior of $G(t)$ at small γ values should not be observed for T away from T_{max} on a more sensitive rheometer.

B. Nonlinear Regime. Flow curves for three different temperatures are shown in Figures 6−8 together

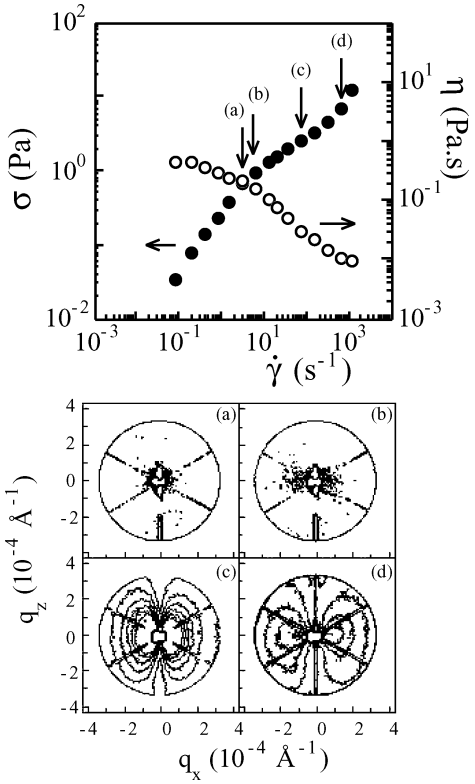

Figure 6. Flow curve measured at $T = 36.7$ °C (top) and representative isointensity plots (bottom) recorded for $\dot{\gamma}$ values indicated by labeled arrows in the top part. Crossing lines at ca. $(2n + 1)\pi/4$ ($n = 0, 1, 2, 3$) are the traces of the nylon threads supporting the beam stop.

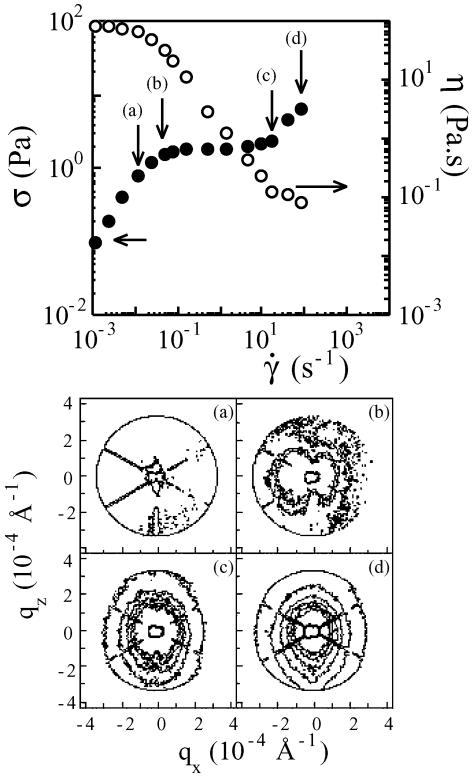

Figure 7. As in Figure 6 for $T = 40.6$ °C.

with some isointensity plots measured at the shear rate values indicated by labeled arrows in the corresponding flow curves. Different regimes can be distinguished in the flow curves according to the shear rate and tem-

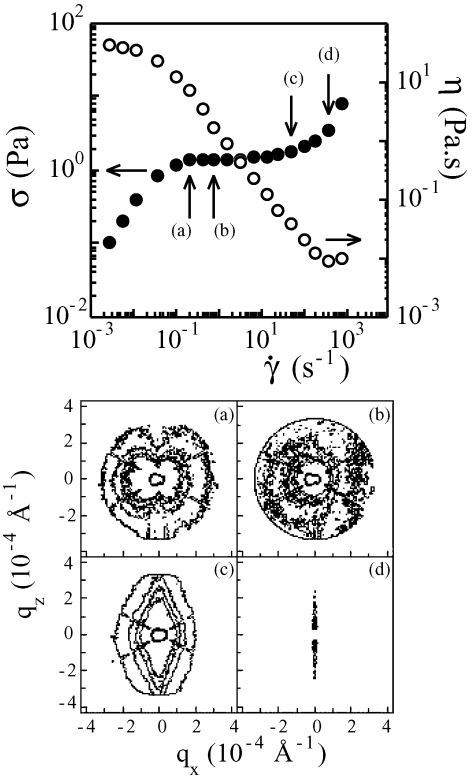

Figure 8. As in Figure 6 for $T = 42.5$ °C.

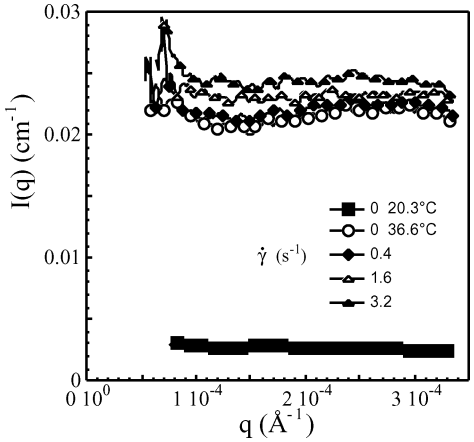

Figure 9. Isotropically averaged scattering intensities measured at $T = 36.7$ °C for $\dot{\gamma}$ values in the Newtonian regime. One point out of 10 is figured.

perature values. For low shear rates, whatever the temperature, the behavior is Newtonian, with the shear viscosity η being nearly constant. In this regime, the scattering intensity remains isotropic and keeps the same average value as in the rest state. A very weak dependence on the scattering wavevector, at the limit of the experimental accuracy, can be observed and will be discussed later. This regime extends up to $\dot{\gamma}\tau \approx 1$, where τ is the longest relaxation time measured in the step strain experiments as described above.

For larger shear rates, shear thinning appears and is accompanied by a butterfly pattern, with the wings oriented along the flow direction. For temperatures above 37.7 °C, this regime is very soon followed by a plateau behavior in the $\sigma(\dot{\gamma})$ curves (Figures 7 and 8). This plateau is not observed for temperatures below 37.7 °C (Figure 6). Whatever the temperature, the scattering intensity increases with the shear rate, which allows us to discard a slip at the walls to be responsible for the plateau behavior.

Finally, for still higher shear rates (typically $\dot{\gamma} > 10$ s^{-1}), the shear stress increases again with shear rate. A significant increase in the fluctuations of the measured stress is observed since the ratio of the standard deviation to the mean value increases by a factor about 10. A bright streak pattern oriented in the direction perpendicular to the flow appears in the scattering intensity. The aspect of this streak depends on temperature. For T below 37.7 °C, a weak streak superposes onto the butterfly pattern (Figure 6d) at the $\dot{\gamma}$ value where a change in the slope of σ vs $\dot{\gamma}$ is observed (Figure 6). For higher temperatures, the streak is more intense and shows fluctuations in both its intensity and its direction. These fluctuations are visible on individual frames, but when the ensemble-average intensity is considered, they are averaged out and the scattering pattern appears as an ellipse oriented perpendicular to the flow (Figure 7c,d). The ellipticity tends to increase with the shear rate, and usually, for these temperatures, the ellipse does not coincide with the butterfly pattern. However, Figure 7c shows a pattern that by chance exhibits a butterfly at low q values while an ellipse at larger q values is clearly distinguished. We may suppose that, for each temperature, such a pattern could be observed if the density of data points was increased. This point is left for future investigation.

When the temperature is increased above T_{max}, the same trends are kept, except that the ellipse seems to appear already in the plateau regime. After the takeoff of the shear stress, a lozange pattern appears (Figure 8c), followed by a very well-defined streak that shows clear bright spots (Figure 8d).

To be more quantitative, Figure 9 shows the averaged isotropic scattering intensities in the quiescent state and in the Newtonian regime for $T = 36.7$ °C. The scattering intensity in the quiescent state at 20 °C is also shown for comparison. It shows a very small negative slope, consistent with small spherical micelles with a radius of the order of 200−300 Å[14] possibly coexisting with some remaining unimers. Upon temperature increase at 36.7 °C, the average scattering intensity increases by a factor 10, a weak and broad maximum at $q \approx 2.7 \times 10^{-4}$ Å^{-1} appears, and some upturn in the scattering intensity at the smallest q values is visible. These features are consistent with the growth of the micelles into larger objects. The q dependence shows however that the structure of the solution is not identical to that of flexible chains in a semidilute solution. A large size polydispersity for the aggregates could explain that the solution is not homogeneous beyond some characteristic length scale. In Figure 9, we have also plotted as a thick line the scattering intensity after the cessation of flow ($\dot{\gamma} = 1280$ s^{-1}). We have constantly observed in the whole investigated temperature range that the scattering intensity relaxes in a few seconds after the cessation of flow to the level measured before the onset of any shear. Although some changes can sometimes be noticed at very small q values, when considering the large anisotropy and intensity increase generated by the flow (see below), we can say that the solutions always return very fast to their pre-shear state after the cessation of flow, at least on the length scales probed by the SALS experiment. From Figure 9, it is also clear that the scattering intensity is almost not affected by the flow in the Newtonian regime, showing at most a 10%

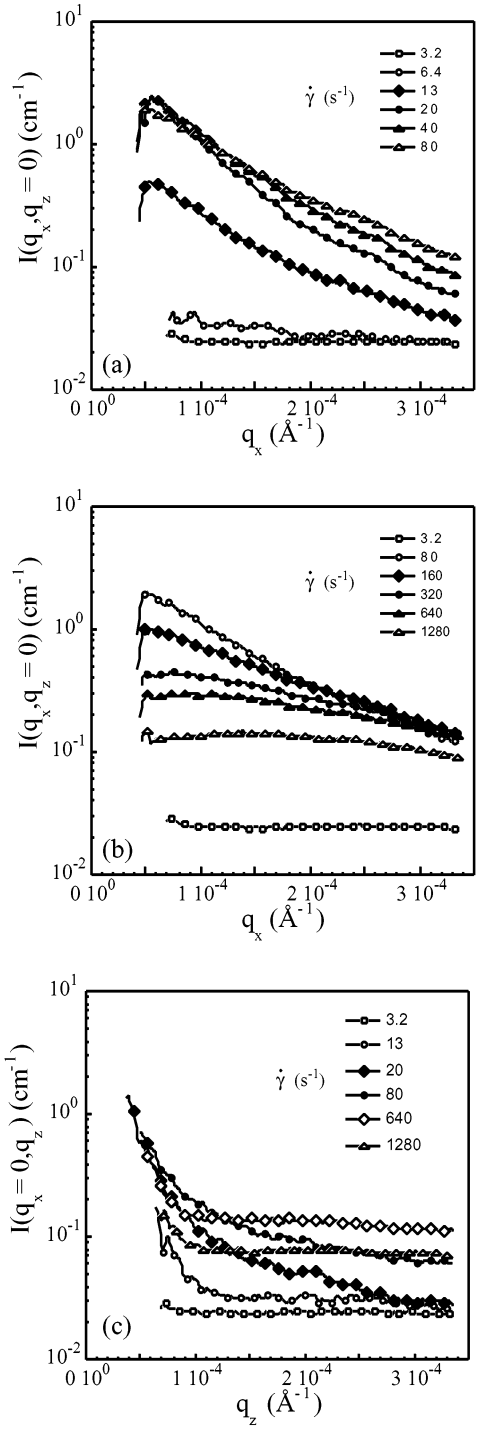

Figure 10. Azimuthally averaged ($\Delta\psi = \pm 5°$) scattering intensities in the direction parallel (a, b) and perpendicular (c) to the flow, measured at T= 36.7 °C for $\dot{\gamma}$ values in the nonlinear regime. One point out of 10 is figured.

increase for $\dot{\gamma} = 3.2$ s^{-1}, at the kink of the flow curve when shear thinning appears (arrow a in Figure 6).

The behavior changes drastically at higher shear rates. Figure 10 shows the evolution with shear rate of the azimuthally averaged ($\Delta\psi = \pm 5°$) scattering intensities in the direction parallel (Figure 10a,b) and perpendicular (Figure 10c) to the flow for $T = 36.7$ °C.

In the direction parallel to the flow, the scattering intensity starts to increase (Figure 10a) at small q values ($\dot{\gamma} = 6.4$ s^{-1}) and then in the whole q range up to 20 s^{-1}. In the range $20 \leq \dot{\gamma}$ (s^{-1}) ≤ 80, the intensity at small q has reached a maximum value about 100 times larger than at rest, while it is still increasing at larger q values. For still higher $\dot{\gamma}$ values, corresponding to the onset of the third regime (Figure 6, arrow c), a decrease of the intensity in the direction parallel to the flow is observed, starting again in the small q region and extending progressively to the whole investigated q range (Figure 10b).

In the direction perpendicular to the flow, the same trend is observed (Figure 10c), although shifted to higher shear rate values. Again the increase is observed first in the small q range, then extends to the whole q window, and reaches a maximum first at small q values while the increase is still observed at the larger q values. The decrease of the intensity is only observed for the highest shear rate ($\dot{\gamma} = 1280$ s^{-1}).

IV. Discussion

It is now well established that spherical micelles made of symmetrical triblock copolymers in a bad solvent of the middle block can grow into elongated micelles under suitable conditions, which have been rationalized a decade ago.[29] It has been argued that elongated micelles are favored when the diameter of the collapsed core becomes larger than the contour length of the middle block. Since the aggregation number tends to increase with temperature for PEO−PPO−PEO copolymers and to decrease with the length of the PEO chains (due to steric constraints), elongated micelles can be expected at high temperatures in systems where the PEO content is not too high. Direct or indirect experimental evidence for elongated micelles has been obtained for copolymers with block lengths 26−40−26 (P85).[2,5,10,13,19,21,22] Therefore, it can be expected that P84, which has a comparable PPO block and shorter PEO blocks, will also display such a transition at high temperature. In fact, both systems exhibit a small additional endothermal peak[9] between the usual peaks corresponding to the micellar aggregation of unimers (at low T) and to the phase separation (cloud point at high T). For P85, this third peak is well correlated to the onset of elongated micelle characteristics in the scattering intensity. For P84, the third peak corresponds to the initial increase in the relative viscosity[9] and in the zero-shear viscosity (Figure 1). The huge increase of the zero-shear viscosity with temperature can be easily understood if micelles with growing length form a transient network of entangled chains in the solution. On the other hand, Liu et al. were able to interpret successfully[24] the initial raise of the relative viscosity (up to $\eta_r \approx 5$) for salt-free P84 solutions in the same concentration range with a sticky hard-sphere model, the parameters of the model being extracted from independent small-angle neutron scattering experiments. Thus, at higher temperatures, one could expect the formation of a percolating network of sticky spheres. Our results suggest rather that, as the stickiness increases at high T, the spherical micelles fuse together and start to grow. In fact, we could not find any indication for the existence of a yield stress in our system and oscillatory measurements indicate indeed that the system remains a viscoelastic liquid at all the investigated temperatures, without the presence of a plateau for $G'(\omega)$ that would be the signature of a gel. As a remark, one reviewer has raised the question whether salt addition could alter the structure of the micelles and explain the different findings in ref 24 and in this work. No direct structural answer is yet available, but DSC scans on P85[9] and on P84[9,30] in the

presence of varying amount of added salt show clearly that the whole thermograms are simply shifted downward along the temperature axis upon salt addition. Apart from this shift the endothermal peaks retain remarkably their shape, and the peak associated with micellar growth is always present. Therefore, we believe that the difference between the two works is simply a matter of working in different regimes of the micellar aggregation.

However, the analogy with entangled polymer solutions has clearly some limits. First, the presence of a maximum in the viscosity (Figure 1) shows that an additional mechanism to micellar growth comes into play above T_{max}. A similar behavior has been observed for the viscosity of small surfactant systems as a function of added salt concentration.[31] It has been argued that if the energy of the hemispherical caps keeps to grow with added salt, then the formation of branches and a viscosity decrease could be expected.[31] The same trend could hold true in the present case if the energy of the end caps of our micelles is an increasing function of temperature. Second, as seen above, the damping function $h(\gamma)$ measured for these solutions does not agree with the one known to describe polymer solutions. This feature indicates that the orientational tensor describing the orientation of statistical units does not vary upon sudden deformation like for flexible polymers. The earlier departure from linear behavior would be indicative of a larger initial stretching in the case of polymer chains. This is hardly conceivable for our bulky cylindrical aggregates. It is more likely that the behavior of $h(\gamma)$ here reflects, at least partly, the living character of the aggregates. Indeed, the early appearance of similar nonlinear effects has been reported as well for surfactant solutions.[28]

The variation of the plateau modulus with temperature, deduced from the data in Figure 4, is also a feature unexpected for usual entangled polymer solutions, for which it scales[27] as $G_0/kT \sim c(b/a)^2$, where kT is the thermal energy, c the concentration, b the length of the statistical units of the chains, and a the diameter of the confining tube. Therefore, within the analogy with entangled polymer solutions, the experimental variation of G_0 with T should be mainly due to an evolution of the ratio b/a. A temperature-dependent rigidity of the aggregates could explain this evolution. A detailed verification of this hypothesis is left for future work.

Finally, we can remark that, although these aggregates are in principle living polymers, $G'(\omega)$ vs $G''(\omega)$ plots (Cole−Cole plots) do not look like semicircles; i.e., the solutions are not Maxwellian. This would mean that we are not in a regime where the breaking time τ_b of the aggregates is much smaller than the reptation time,[32] in agreement with known results about the kinetics of similar systems.[33−35] Therefore, the dynamics of the stress relaxation as measured by our τ values should be dominated by the disengagement of entangled aggregates. The fact that $G(t)$ could be approximated as a single exponential (plus baseline) at $T = 40.5$ °C (see above) might indicate that, at that temperature, the cylindrical micelles are long enough to meet the requirement of a reptation time much longer than the breaking time. But, as mentioned above, the experiments in the linear regime were noisy, and the oscillatory measurements were also performed at the limits of the experimental sensitivity. Clearly additional work with a more sensitive apparatus and with additional techniques is needed before a firm conclusion can be reached on this point. We now turn to the complex behavior in the nonlinear regime.

For $T < 37.7$ °C, the flow curves $\sigma(\dot\gamma)$ display a monotonic increase of the shear stress with the shear rate. But the slope $d(\log \sigma)/d(\log \dot\gamma)$ shows distinct changes in its value that are correlated with qualitatively different scattering intensity patterns. We can distinguish the Newtonian regime, a second regime where the scattering patterns display butterfly shapes and a third regime where a bright streak superposes to the butterfly pattern. We discuss the scattering intensity in more details later on.

For temperatures higher than 37.7 °C, the flow curves become qualitatively different. After the Newtonian regime, the second regime corresponds now to a plateau behavior for increasing shear rate, with a constant stress of the order of the plateau modulus G_0. In this regime, the isointensity plots display a butterfly pattern, and the general trend is an increase of the scattering intensity with $\dot\gamma$. This allows us to exclude slip at the walls and to believe that this plateau is the signature of gradient shear banding,[36,37] with the shear velocity gradient having a nonconstant value across the gap. Moreover, the fact that the plateau value in this nonlinear regime is comparable with the plateau modulus G_0 is an additional argument in favor of shear banding.[37] The third regime is distinguished by a new increase of the stress with $\dot\gamma$ and scattering patterns that are either fluctuating streaks averaging out as ellipses (below T_{max}) or well-defined spotted streaks (above T_{max}). The presence of gradient shear banding implies that the total scattering intensity is a complex signal superposing the contributions from bands with different shear velocity gradients. To separate these contributions, it is crucial to measure the velocity field across the gap. This work is still in progress, and we therefore postpone the analysis of these intensity patterns to a later paper. For the present, we just propose some preliminary hypotheses.

Starting from the fact that T_{max} is not far from the cloud point temperature, it is likely that the scattering intensity increase reflects the now well-documented shear-induced phase separation,[38−44] which originates from the dynamic coupling between stress and diffusion close to a phase transition boundary. Indeed, the fact that the streak pattern becomes more and more defined as we approach the vicinity of the cloud point supports this idea. Thus, the spotted streak at 42.6 °C and high shear rates (Figure 8d) would be the signature of a highly ordered phase generated by the flow close to the cloud point. For lower temperatures, this ordering would be less easy, with higher shear rates needed to generate the first aligned regions. This is consistent with the trend for ellipse patterns to appear at lower $\dot\gamma$ values as temperature is increased above T_{max}. This shear-induced phase separation appears linked to a shear banding phenomenon, i.e., to a coexistence of phases with different $\dot\gamma$ and, therefore, different structures. If this sketchy picture is correct, this system would be, as far as we know, the first example where the shear banding phenomenon and the associated phase transition are controlled through the temperature and the flow. For short surfactant micellar systems, the other control parameter, besides the flow, is usually the surfactant concentration (for a review, see for instance ref 44) and sometimes the salt concentration.[45] These

hypotheses will be explored in detail in future work. In the following, we focus on the intensity curves measured at 36.7 °C, where no plateau is observed in the flow curves (Figure 6).

Clearly the evolution depicted in Figures 9 and 10 is only a shortcut that reflects poorly the complex evolution of the anisotropy pattern in the isointensity plots (Figure 6). Thus, a satisfying interpretation of the system behavior should be based on the evolution of the whole isointensity pattern. This requires both a dynamic equation for the concentration fluctuations, accounting for the dynamic coupling between stress and diffusion, and an adequate constitutive equation, accounting for the nonlinear rheological behavior of the solution. Such a model has been proposed recently by Saito et al.[43] They used the dynamical equation for concentration fluctuations proposed by Helfand−Fredrickson,[38] Milner,[41] and Onuki[42] (HFMO), together with the Kaye−BKZ constitutive equation,[46] to investigate the shear-flow properties of semidilute solutions of polystyrene in dioctyl phthalate. Interestingly, this model predicts for the q_z direction (normal to the flow) either no intensity increase (normal stresses turned off) or a weak intensity decrease (normal stresses turned on).[43] Thus, its domain of validity would be anyway limited to shear rates below 6.4 s^{-1} for our system at 36.7 °C (Figure 10c), a range where we have not for the present enough data.

For semidilute polystyrene solutions, a large increase of the scattering intensity in the z direction has also been reported and attributed to the convection by the flow of phase-separated structures.[43] This would explain the failure of a theory based on the linearization of the concentration fluctuations. That a similar regime is observed in our system is a supplementary argument for the existence of a shear-induced phase separation, suggesting moreover that, above $\dot{\gamma} = 6.4\ s^{-1}$, the system is no longer in the regime of shear-enhanced concentration fluctuations but has already entered the regime where separated phases coexist. However, since such a phase separation seems correlated to shear banding at higher temperatures, the Kaye−BKZ constitutive equation that does not allow such a phenomenon is probably not the best candidate for a constitutive equation in our case. Very recently, Fielding and Olmsted worked out a model that includes the dynamic coupling between stress and concentration fluctuations and also predicts shear banding for certain conditions.[44,47] This appears as a very appealing model to compare with our experimental results. Clearly, much effort is worth doing in this direction and will be attempted in future work.

V. Conclusions

The dilute aqueous solutions of P84 with added salt show a spectacular increase (5 orders of magnitude) of the zero-shear viscosity upon a temperature increase from 30 °C to about 40.5 °C. Above this temperature, η_0 decreases with temperature before reaching the cloud point of the solution at about 43 °C. In the whole temperature range where oscillatory measurements are feasible, the behavior of the storage and loss moduli indicate that the system remains a viscoelastic liquid. The linear rheology of these solutions is consistent with an entangled solution of polydisperse cylindrical aggregates, where the kinetics of breaking and recombination are slow compared to the disengagement time τ of the micelles.

Close to the region of maximum viscosity, the flow curves $\sigma(\dot{\gamma})$ exhibit a plateau, which suggests gradient shear banding, i.e., the coexistence of regions with different shear rate values across the gap, in the non-Newtonian regime $\dot{\gamma}\tau > 1$. The SALS experiments show a complex anisotropy pattern, whose evolution is correlated with the different regimes identified in the flow curves. At high shear rates, streak patterns indicate an ordering of the system by the flow. This ordering appears easier and better as the cloud point is approached.

Below the critical temperature, when σ still increases steadily with $\dot{\gamma}$, the scattering intensity increases markedly with the shear rate, until a weak streak pattern develops and the scattering intensity decreases. This behavior can be understood qualitatively in terms of shear-induced demixing, i.e., by the enhancement of concentration fluctuations through the dynamic coupling between stress and diffusion.

Thus, this system appears as an interesting example, where, above a critical temperature, the shear-induced demixing triggered by the flow in the vicinity of the cloud point is linked to a macroscopic phase separation of regions with different shear rates. The control parameters of this dynamic phase diagram are the temperature and the flow.

Future work will investigate the velocity profiles across the gap and make attempts for quantitative comparison with adequate models recently published.

References and Notes

(1) See, e.g.: Kozlov, M. Y.; Melik-Nubarov, N. S.; Batrakova, E. V.; Kabanov, A. *Macromolecules* **2000**, *33*, 3305 and references therein.
(2) Mortensen, K.; Brown, W. *Macromolecules* **1993**, *26*, 4128.
(3) Wanka, G.; Hoffmann, H.; Ulbricht, W. *Colloid Polym. Sci.* **1990**, *268*, 101.
(4) Chowdhry, B.; Leharne, S.; Mitchell, J.; Beezer, A.; Lohner, K.; Laggner, P. *J. Phys. Chem.* **1993**, *97*, 3904.
(5) Beezer, A.; Loh, W.; Mitchell, J.; Royall, P.; Smith, D.; Tute, M.; Parsonage, J.; Armstrong, J.; Chowdhry, B.; Leharne, S.; Eagland, D.; Crowther, N. *Langmuir* **1994**, *10*, 4001.
(6) Hvidt, S.; Jørgensen, E. B.; Brown, W.; Schillén, K. *J. Phys. Chem.* **1994**, *98*, 12320.
(7) Patterson, I.; Chowdhry, B.; Leharne, S. *Colloids Surf. A* **1996**, *111*, 263.
(8) Alexandridis, P.; Holzwarth, J. F. *Langmuir* **1997**, *13*, 6074.
(9) Michels, B.; Waton, G.; Zana, R. *Colloids Surf. A: Physicochem. Eng. Aspects* **2001**, *183−185*, 55.
(10) Glatter, O.; Scherf, G.; Schillén, K.; Brown, W. *Macromolecules* **1994**, *27*, 6046.
(11) Mortensen, K.; Pedersen, J. S. *Macromolecules* **1993**, *26*, 805.
(12) Berret, J.-F.; Molino, F.; Porte, G.; Diat, O.; Lindner, P. *J. Phys.: Condens. Matter* **1996**, *8*, 9513.
(13) King, S. M.; Heenan, R. K.; Cloke, V. M.; Washington, C. *Macromolecules* **1997**, *30*, 6215.
(14) Liu, Y.; Chen, S.-H.; Huang, J. S. *Macromolecules* **1998**, *31*, 2236.
(15) Eiser, E.; Molino, F.; Porte, G.; Pithon, X. *Rheol. Acta* **2000**, *39*, 201.
(16) Eiser, E.; Molino, F.; Porte, G.; Diat, O. *Phys. Rev. E* **2000**, *61*, 6759.
(17) Mortensen, K. *Colloids Surf. A: Physicochem. Eng. Aspects* **2001**, *183−185*, 277.
(18) Pedersen, J. K.; Svaneborg, C. *Curr. Opin. Colloid Interface Sci.* **2002**, *7*, 158.
(19) Brown, W.; Schillén, K.; Almgren, M.; Hvidt, S.; Bahadur, P. *J. Phys. Chem.* **1991**, *95*, 1850.
(20) Liu, Y.; Chen, S.-H.; Huang, J. S. *Macromolecules* **1998**, *31*, 6226.
(21) Schillén, K.; Brown, W.; Johnsen, R. M. *Macromolecules* **1994**, *27*, 4825.
(22) Jørgensen, E. B.; Hvidt, S.; Brown, W.; Schillén, K. *Macromolecules* **1997**, *30*, 2355.
(23) Chen, S. H.; Mallamace, F.; Faraone, A.; Gambadauro, P.; Lombardo, D.; Chen, W. R. *Eur. Phys. J. E* **2002**, *9*, 283.

(24) Liu, Y.; Chen, S.-H.; Huang, J. S. *Phys. Rev. E* **1996**, *54*, 1698.
(25) Weber, V.; Schosseler, F. *Rev. Sci. Instrum.* **2002**, *73*, 2537.
(26) Osaki, K.; Kurata, M. *Macromolecules* **1980**, *13*, 671.
(27) Doi, M.; Edwards, S. F. *The Theory of Polymer Dynamics*; Clarendon Press: Oxford, 1986.
(28) Callaghan, P. T.; Cates, M. E.; Rofe, C. J.; Smeulders, J. B. A. F. *J. Phys. II* **1996**, *6*, 375.
(29) Linse, P. *Macromolecules* **1993**, *26*, 4437.
(30) Michels, B.; Waton, G., unpublished results.
(31) Candau, S. J.; Khatory, A.; Lequeux, F.; Kern, F. *J. Phys. IV* **1993**, *3*, 197.
(32) Cates, M. E. *Macromolecules* **1987**, *20*, 2289.
(33) Waton, G.; Michels, B.; Zana, R. *Macromolecules* **2001**, *34*, 907.
(34) Willner, L.; Poppe, A.; Allgaier, J.; Monkenbusch, M.; Richter, D. *Europhys. Lett.* **2001**, *55*, 667.
(35) Riess, G. *Prog. Polym. Sci.* **2003**, *28*, 1107 and references therein.
(36) Rehage, H.; Hoffmann, H. *Mol. Phys.* **1991**, *74*, 933.
(37) Cates, M. E.; McLeish, T. C. B.; Marrucci, G. *Europhys. Lett.* **1993**, *21*, 451.
(38) Helfand, E.; Fredrickson, G. H. *Phys. Rev. Lett.* **1989**, *62*, 2468.
(39) Wu, X.-L.; Pine, D. J.; Dixon, P. K. *Phys. Rev. Lett.* **1991**, *66*, 2408.
(40) Hashimoto, T.; Fujioka, K. *J. Phys. Soc. Jpn.* **1991**, *60*, 356.
(41) Milner, S. *Phys. Rev. E* **1993**, *48*, 3674.
(42) Onuki, A. *J. Phys.: Condens. Matter* **1997**, *9*, 6119.
(43) Saito, S.; Takenaka, M.; Toyoda, N.; Hashimoto, T. *Macromolecules* **2001**, *34*, 6461 and references therein.
(44) Fielding, S. M.; Olmsted, P. D. *Eur. Phys. J. E* **2003**, *11*, 65.
(45) Decruppe, J.-P.; Ponton, A. *Eur. Phys. J. E* **2003**, *10*, 201.
(46) Larson, R. G. *Constitutive Equations for Polymer Melts and Solutions*; Butterworth: Boston, 1988.
(47) Fielding, S. M.; Olmsted, P. D. *Phys. Rev. Lett.* **2003**, *90*, 224501.

MA0349332